Ruthenium Oxide Hydrogen Evolution Catalysis on Composite Cuprous Oxide Water-Splitting Photocathodes

S. David Tilley, Marcel Schreier, João Azevedo, Morgan Stefik, and Michael Graetzel*

Photocathodes based on cuprous oxide (Cu_2O) are promising materials for large scale and widespread solar fuel generation due to the abundance of copper, suitable bandgap, and favorable band alignments for reducing water and carbon dioxide. A protective overlayer is required to stabilize the Cu_2O in aqueous media under illumination, and the interface between this overlayer and the catalyst nanoparticles was previously identified as a key source of instability. Here, the properties of the protective titanium dioxide overlayer of composite cuprous oxide photocathodes are further investigated, as well as an oxide-based hydrogen evolution catalyst, ruthenium oxide (RuO_2). The RuO_2-catalyzed photoelectrodes exhibit much improved stability versus platinum nanoparticles, with 94% stability after 8 h of light-chopping chronoamperometry. Faradaic efficiencies of ~100% are obtained as determined by measurement of the evolved hydrogen gas. The sustained photocurrents of close to 5 mA cm^{-2} obtained with this electrode during the chronoamperometry measurement (at 0 V vs. the reversible hydrogen electrode, pH 5, and simulated 1 sun illumination) would correspond to greater than 6% solar-to-hydrogen conversion efficiency in a tandem photoelectrochemical cell, where the bias is provided by a photovoltaic device such as a dye-sensitized solar cell.

1. Introduction

Photoelectrochemical (PEC) water splitting has been achieved with a diverse range of materials since the seminal photoanode demonstrations more than four decades ago.[1,2] This process relies crucially on the stability of a photoactive material in the aqueous environment in concert with effective and stable catalysts for both the hydrogen evolution reaction (HER) and the oxygen evolution reaction (OER).[3,4] The interface between a photoabsorbing material and the catalyst is of great importance. The catalyst should ideally be optically transparent and should form a stable physical and electrical contact at the semiconductor-liquid junction (SCLJ).

Photocathodes based on cuprous oxide, Cu_2O, offer the possibility for widespread employment due to the natural abundance of copper and are thus under active investigation in several laboratories[5–11] including our own.[12,13] We have recently reported on the nature of the multilayer composite photocathodes, which consist of a buried photovoltaic (PV) p–n junction comprised of p-type Cu_2O and n-type Al:ZnO (AZO), with the TiO_2 overlayer serving to protect the PV from the aqueous environment.[14] We investigated the cause of the eventual deactivation of the photocathodes, despite the fact that we have yet to find evidence for the degradation of the Cu_2O material in the composite structures (X-ray diffraction reveals only the Cu_2O phase after long-term stability measurements with the overlayer-protected films, in contrast to unprotected Cu_2O films, which show Cu(0) and Cu(II)O phases that result from photocorrosion due to the direct contact of the electrolyte with the Cu_2O).[12,14] The conclusions of these studies brought our attention to the interface between the TiO_2 and the platinum nanoparticles, serving as a hydrogen evolution catalyst. It was observed that re-platinization of the deactivated electrodes often fully recovered the initial activity. This observation led us to conclude that the adhesion of the platinum nanoparticles to the oxide surface was weak, with the platinum becoming dislodged during photoelectrolysis (a process correlated with accumulation of Ti^{3+} in the TiO_2 overlayer).[12] We hypothesized that minimizing the presence of Ti^{3+} centers in the as-deposited film may increase the stability. Thus, we investigated the use of hydrogen peroxide during the ALD deposition in an effort to ensure that we deposited titanium in the most oxidized 4+ state upon decomposition of the titanium precursor. Additionally, we investigated an alternative method for deposition of the platinum catalyst (e-beam evaporation) as well as a different hydrogen-evolution catalyst (ruthenium oxide) that is more resistant than platinum to poisoning by trace impurities in the electrolyte (heavy metal ion impurities in the buffer salts may plate out on the platinum nanoparticles, reducing their surface area and increasing the overpotential).[15]

Dr. S. D. Tilley, M. Schreier, Dr. M. Stefik, Prof. M. Graetzel
Institut des Sciences et Ingénierie Chimiques
Ecole Polytechnique Fédérale de Lausanne
CH-1015, Lausanne, Switzerland
E-mail: david.tilley@epfl.ch
J. Azevedo
Laboratório de Engenharia de Processos
Ambiente e Energia, Rua Dr. Roberto Frias
4200–465, Porto, Portugal
J. Azevedo
Instituto de Física dos Materiais da Universidade do Porto
Instituto de Nanociência e Nanotecnologia
Rua do Campo Alegre 687, 4169–007, Porto, Portugal.

DOI: 10.1002/adfm201301106

2. Results and Discussion

2.1. Atomic Layer Deposition of TiO_2 Overlayers

In our earlier work, we sought to keep the atomic layer deposition (ALD) TiO_2 protective overlayer as thin as possible as we had sometimes observed reduced photocurrents upon using thicker films when depositing films using titanium tetraisopropoxide and water as the ALD precursors. However, after switching to the tetrakisdimethylaminotitanium (TDMAT) precursor, we discovered that thicker TiO_2 layers did not seem to hurt the plateau photocurrents generated by our devices. This discovery allowed us to explore very thick ALD layers (up to 100 nm) with the aim of extending our device lifetime by reducing the likelihood of pinholes in the protective film. The fact that the thicker (and presumably more resistive) TiO_2 layers gave the same plateau photocurrents was at first surprising. This observation is, however, analogous to the "photo-doping" phenomenon in the dye-sensitized solar cell whereby injected electrons increase the conductivity of the TiO_2 by several orders of magnitude such that very small resistance losses are observed.[16] This finding was recently reported by Seger et al. using sputtered TiO_2 protective layers on silicon-based photocathodes in which the authors observed no impediment to electron transfer through the 100 nm-thick sputtered TiO_2 film.[17]

Unfortunately, high temperature annealing of our multilayer photocathodes in order to improve the crystallinity of the overlayers proves detrimental to the device performance. We therefore sought to limit our heat exposure to 150 °C as we had observed that depositing films of TiO_2 at this temperature under our standard conditions of TDMAT and water yielded photoelectrodes with high photocurrents and greatly enhanced stability.[14]

2.2. Hydrogen Evolution Catalysis with Platinum

After optimization of several parameters related to electrode preparation and the photoelectrochemical cell configuration, which led to vastly improved onset potential and fill factor for our photocathodes (see Experimental Section and Figure S1), we explored the parameter space surrounding the TiO_2/catalyst interface. In addition to our standard dark electrodeposition of platinum catalyst, we investigated both photoelectrodeposition and e-beam evaporation of platinum. **Figure 1** depicts a schematic representation, a cross-sectional scanning electron microscopy (SEM) image, and the J–V characteristics of a photocathode that was prepared using 100 nm of TiO_2 deposited using H_2O_2 as the oxygen precursor and with an e-beam evaporated Pt catalyst layer (nominally 1 nm). We observed an onset potential of +0.55 V versus the reversible hydrogen electrode (RHE), nearly 4 mA cm^{-2} of photocurrent at +0.4 V/RHE and a plateau photocurrent of greater than 6 mA cm^{-2} at 0 V/RHE. Ultimately, it is the photocurrent density at the low reverse bias potentials that are the most interesting for tandem cell applications.[18] The oxidative currents at more positive bias potentials (around +0.45 V/RHE) that are observed during the dark phase of the light chopping are due to oxidation of hydrogen that was created during the illuminated phase of the light chopping. This hypothesis was supported by directing a stream of electrolyte at the electrode surface with a pipette just prior to the dark phase of the light chopping in order to remove the hydrogen bubbles, which eliminated the oxidative currents. At more negative bias potentials (+0.1 V/RHE), there is less of a driving force for hydrogen oxidation and no oxidative dark current is observed.

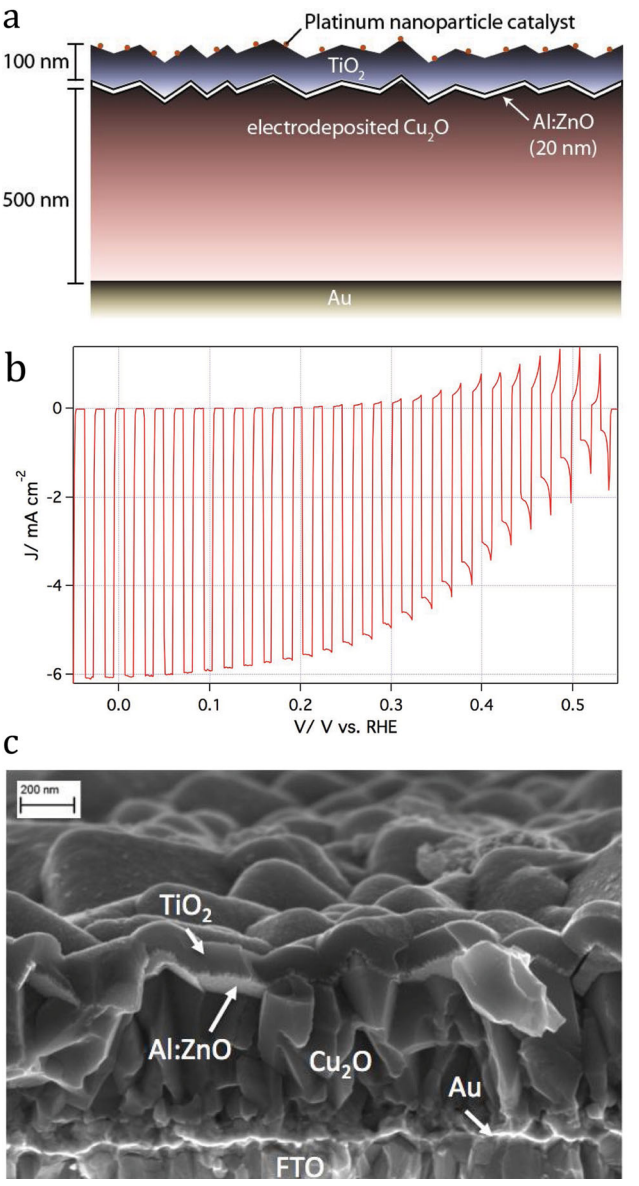

Figure 1. a) The architecture of the photocathode. ALD layers are deposited atop an electrodeposited Cu_2O film, followed by catalyst deposition. b) Current–voltage characteristics under light chopping (in pH 5.0 phosphate–sulfate electrolyte) of such a photocathode in which the Pt catalyst was deposited by e-beam evaporation (nominally 1 nm). c) Cross-sectional SEM micrograph of this photocathode with as-deposited ALD layers.

The stability measurement of this composite photocathode, carried out under light chopping conditions, was typical of our Pt-catalyzed electrodes (regardless of the method of catalyst deposition) with a somewhat rapid decrease of photocurrent during

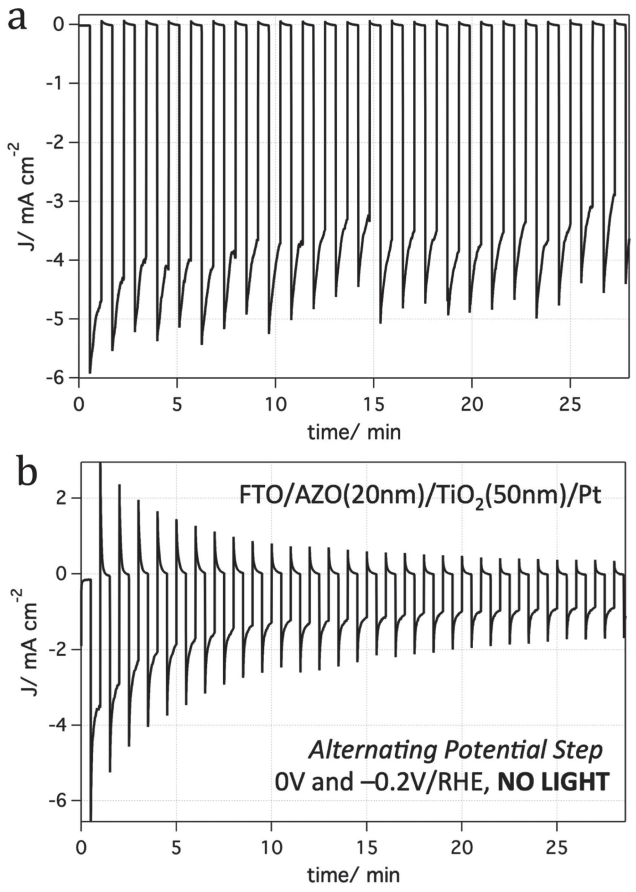

Figure 2. a) Typical chronoamperometry measurement of a Pt-catalyzed photocathode, biased at 0 V/RHE in pH 5.0 phosphate–sulfate electrolyte under light chopping. A rapid decrease in photocurrent is observed during the 30 second light phase that is mostly recovered during the dark phase. b) Potential step experiment of an FTO electrode that was coated with the overlayers and then platinized in order to simulate the light chopping in the PEC experiment. The same trend is observed, suggesting that the Cu_2O is not the source of the instability.

the light phase that mostly recovers after the dark phase of the light chopping (**Figure 2**a). We have attributed this behavior to depletion of protons close to the electrode surface during illumination, followed by electrolyte re-equilibration during the dark phase. Over longer time scales, the average photocurrent decreases as well, which we attribute to irreversible loss of Pt from the electrode surface. However, in order to eliminate the possibility that this longer timescale decrease is due to a changing output voltage of the p–n junction (due to instability of the Cu_2O), we investigated the overlayer/catalyst structure deposited directly onto FTO and simulated the light chopping by using potential step chronoamperometry at voltages that gave similar currents to the photocurrents typically observed with the cuprous oxide photocathodes. Thus, platinized AZO/TiO_2 deposited on FTO was subjected to alternating bias voltages of 0 V and –0.2 V/RHE on the same time scale as the light chopping experiments (every 30 s). As can be seen from Figure 2b, the same general phenomenon is observed: a rapid decrease in current during the higher voltage step that is partially recovered after the lower voltage rest period. Additionally, the overall reduction in higher voltage current over longer time scales is similarly observed. This observation provides further evidence that the deactivation of the (photo)cathode is due to the Pt nanoparticles/overlayers and not due to the Cu_2O absorber material.

2.3. Hydrogen Evolution Catalysis with Ruthenium Oxide

We next sought to investigate a catalyst that might interface better with the TiO_2 overlayer and is more robust to poisoning by trace impurities in the electrolyte. Ruthenium dioxide (RuO_2), perhaps best known as an effective water oxidation catalyst, is also a very effective hydrogen evolution catalyst.[19] For a current density of 10 mA cm^{-2}—a realistic value of what one could obtain with a 2 eV bandgap (Cu_2O) and AM 1.5 solar illumination—RuO_2 requires only an additional 30 mV of overpotential compared to Pt, the best known hydrogen-evolving catalyst.[15] Additionally, the fact that RuO_2/TiO_2 is used industrially for chlorine evolution (the De Nora catalyst[20]) led us to believe that we could expect a robust binding between RuO_2 and the TiO_2 overlayer of our photocathode. In order to load the catalyst onto the surface, we modified a literature procedure for loading RuO_2 onto TiO_2 particles whereby the particles were irradiated with UV light in the presence of $KRuO_4$ and a hole scavenger, and RuO_x was formed via reduction of the perruthenate anions by conduction band electrons generated by photoexcitation of the TiO_2.[21] For our system, we simply supplied the TiO_2 with electrons from the potentiostat and used light to get an idea of the photovoltage generated by our p–n junction (the current density for catalyst deposition is sufficiently small that cathodic currents can be passed in the dark at relatively low voltages, i.e. voltages that are insufficient for water reduction, see Figure S3).

We deposited RuO_x galvanostatically in the dark onto an FTO electrode that had been coated with AZO and TiO_2. Again, we simulated light chopping in this dark experiment by using potential step chronoamperometry at voltages that gave similar currents to the photocurrents typically observed with the cuprous oxide photocathodes. As can be seen from **Figure 3**,

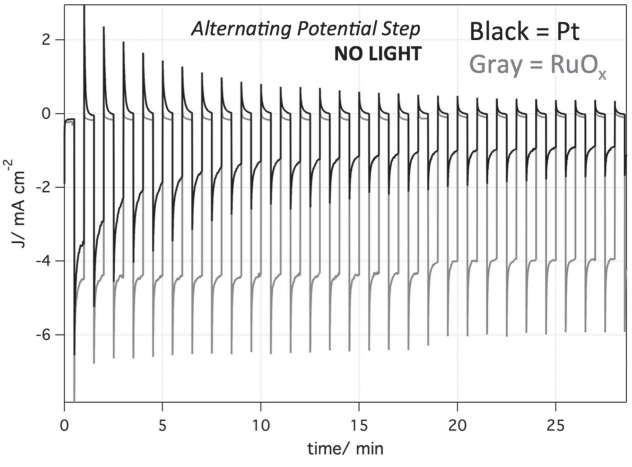

Figure 3. Potential step experiment in pH 5.0 phosphate–sulfate electrolyte of an FTO electrode coated with the ALD overlayers and a Pt or RuO_x catalyst in order to simulate the light chopping in the PEC experiment. The RuO_x catalyst exhibits much improved stability.

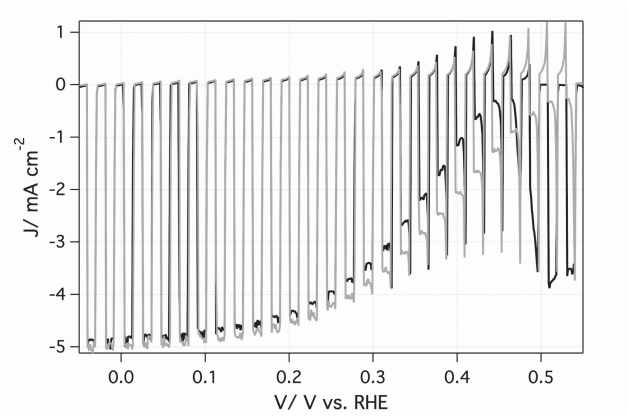

Figure 4. Current–voltage characteristics in pH 5.0 phosphate–sulfate electrolyte of a composite photocathode with RuO_x catalyst. The first linear sweep (black trace) exhibits a strong photoreduction current in the first seconds, indicating activation of the photoelectrodeposited catalyst. Subsequent sweeps show an improved onset potential (gray trace).

the electrode is much more robust using the RuO_x catalyst. We observe a transient during the higher bias phase but the global decrease is not observed (the small step decrease at ~18 min in the RuO_x curve is likely due to a trapped hydrogen bubble and subsequent loss of surface area).

We then experimented with addition of the RuO_x catalyst to our composite photocathodes. Again, we used the galvanostatic photodeposition technique to get an idea of the photovoltage generated by our p–n junction (Figure S3). After deposition of the ruthenium oxide catalyst, the electrode surface was visibly darker, yet the plateau photocurrents were not drastically reduced. As can be seen in **Figure 4**, the first linear sweep yields a strong reduction photocurrent in the first three light chops that we attribute to reduction of the deposited RuO_x species on the surface to form the active catalyst. This activation phenomenon is well known for RuO_2 electrodes.[19] It is only after the formation of active catalyst that hydrogen is generated as evidenced by the oxidation currents in the dark phase at more positive bias, where the driving force for hydrogen oxidation (in the dark) is high. After catalyst activation, we observe an onset at +0.55 V/RHE and plateau photocurrents of 5 mA cm^{-2} (slightly reduced due to light absorption by the catalyst). We also observe an improved fill factor that enables photocurrents of 4 mA cm^{-2} at +0.3 V/RHE.

This photocathode yielded vastly improved long-term photocurrent characteristics with 94% of photocurrent remaining after 8 hours of light chopping when biasing at 0V/RHE (**Figure 5**a). Contrary to the Pt nanoparticle catalyst, we did not observe the severe decrease during the light phase of the chopping (Figure 5b), nor did we observe the general long term decrease over several hours. The somewhat noisy photocurrent at around 5 mA cm^{-2} is due to bubble evolution on the surface of the photocathode and accumulation of the smaller bubbles within the aperture of the PEC cell that eventually escape as the bubble size increases.

We quantified the amount of RuO_x that was deposited using this electrodeposition method by atomic absorption spectroscopy (AAS) of digested films. Longer deposition times of the same current density used in the photocathode experiments

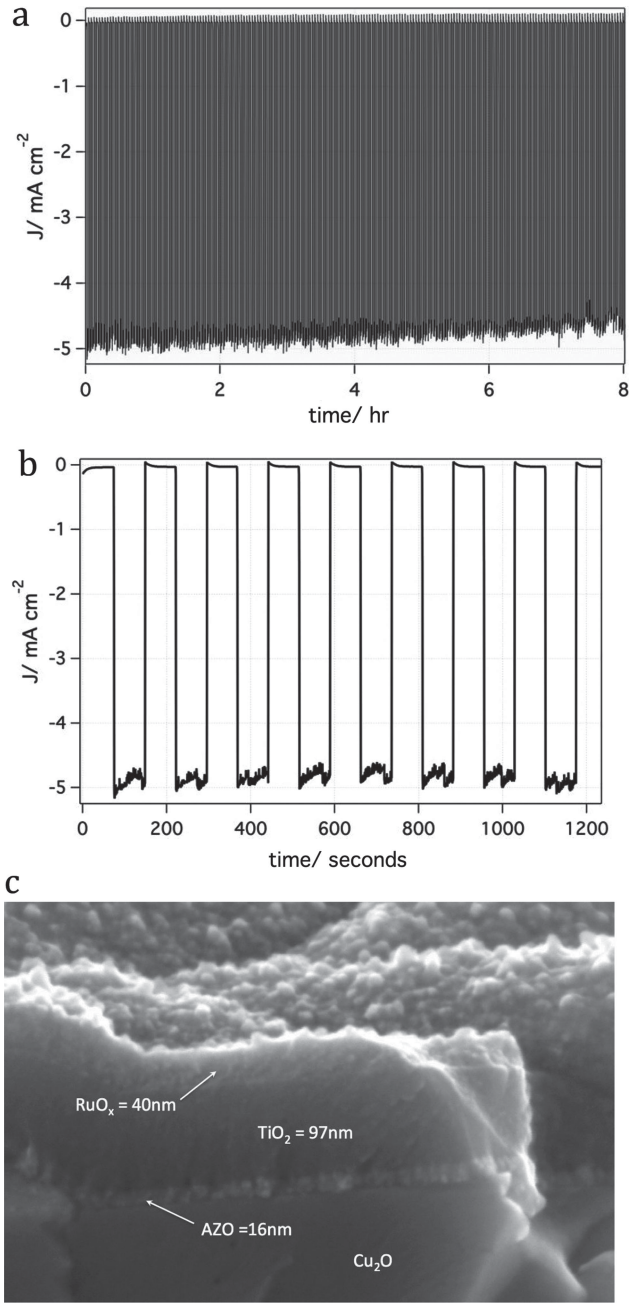

Figure 5. a) Chronoamperometric stability measurement of the photocathode of Figure 4, biased at 0 V/RHE in pH 5.0 phosphate–sulfate electrolyte under light chopping. This electrode exhibits 94% stability after 8 h of measurement. b) The photocurrent is stable during the light phase of the chopping: the small variations are due to gas bubble evolution, trapping (loss of surface area), and eventual escape (surface area recovered). c) Cross-sectional SEM micrograph of the electrode after the stability measurement, revealing a conformal, porous catalyst layer atop the TiO_2 protective layer.

were used in order to produce a signal above the detection limit of the instrument (see Supporting Information). In this way we determined a Faradaic efficiency of the electrodeposition of 16 ± 5%, assuming 3 electrons per Ru atom (Ru^{7+} in the $KRuO_4$ precursor goes to Ru^{4+} in RuO_2).

Based on the amount of current passed during the electrodeposition of catalyst on our photocathodes, the Faradaic efficiency obtained from AAS, and the density of crystalline RuO_2 (6.97 g cm^{-3}), we would expect a ~3 nm thick layer of RuO_2 if it were in fact crystalline. In practice, the deposited catalyst will be a hydrous, amorphous layer and therefore much less dense. Cross-sectional SEM of the photocathode measured after the stability measurement shows that the catalyst layer is roughly 40 nm thick and conformally coats the surface (Figure 5c). Cross-sectional SEM on this and several other samples prepared under these same conditions appears to show a very porous catalyst layer. The errors incumbent in the AAS measurement (see Supporting Information) and the porosity of the film are the reason for the unexpected thickness of the catalyst layer as revealed by cross-sectional SEM. More sensitive techniques for the detection of the minute quantities of catalyst used in these experiments will be applied in the future in order to better quantify the catalyst loading of optimized photocathodes.

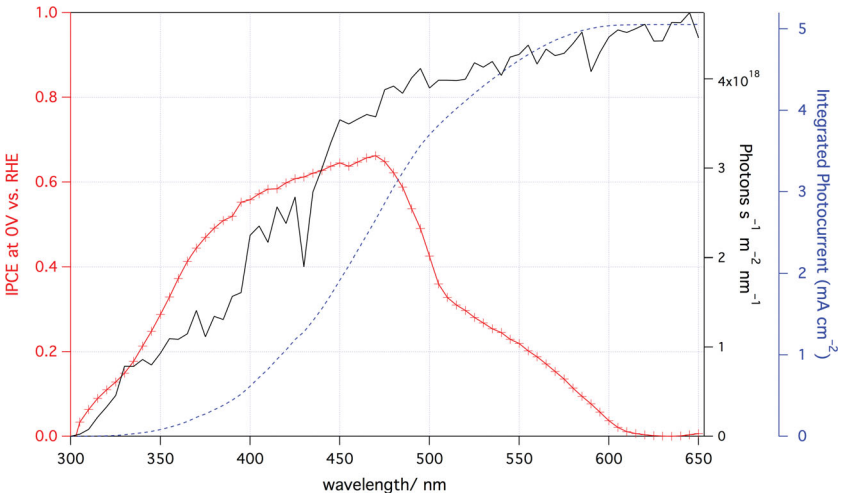

Figure 6. Incident-photon-to-current-efficiency (IPCE) of a photocathode with RuO_x catalyst biased at 0 V/RHE in standard pH 5 electrolyte. Integration of the IPCE values with the solar AM 1.5 spectrum gives the same photocurrent value as is typically observed with our simulated one sun illumination.

It is clear, however, that the catalyst loading is higher with RuO_x than with Pt. As previously observed,[12,14] the quantity of platinum that is deposited is too small to be seen by SEM and the calculation for what one would expect (assuming unity Faradaic efficiency as an upper limit) is approximately 1.7 nm. No effort was made to exclude oxygen from the electrodeposition solution (equally for the RuO_x precursor solution) and so we would expect a much lower Faradaic efficiency and therefore less deposited platinum. It is perhaps because of the porous nature of the RuO_x catalyst that we do not observe the steep decrease in photocurrent during the illuminated phase of the light chopping that we observe with the platinum: the depletion of protons in the electrolyte is much less severe with the increased surface area provided by the porous catalyst layer. Additionally, if the catalyst particles within the RuO_x layer exhibit a spherical morphology, the diffusion layer that develops due to the proton reduction is limited, thus facilitating the diffusion of protons to the electrode surface and therefore sustaining relatively high current densities (in analogy with spherical ultramicroelectrodes). This is in contrast to a planar electrode where the diffusion layer continues to grow throughout the electrolysis. As we only observe a very minor decrease in photocurrent under conditions of vigorous bubble evolution, it appears that molecular hydrogen is able to diffuse out of the porous catalyst layer prior to bubble formation. Bubble formation within the small pores is disfavored as this would require the displacement of water from the hydrophilic surface of the catalyst.

2.4. Photoresponse and Faradaic Efficiency

In an effort to understand how to improve the photoresponse of our device, we analyzed the incident photon-to-current efficiency (IPCE) of our stable photocathode (**Figure 6**). In the visible region between 420 and 470 nm, we observe IPCE values in excess of 60%. The IPCE values decrease towards the ultraviolet region due to unproductive absorption by the 100 nm TiO_2 overlayer. The precipitous drop in the IPCE at 480 nm points to a clear path forward for increasing the photocurrent of our system by improving productive absorption in the range 480–600 nm. Importantly, the integration of the IPCE values with the solar AM 1.5 spectrum yields 5.0 mA cm^{-2}, validating our light source for true AM 1.5 solar simulation.

We calculated the losses entailed by absorption/reflection of the RuO_x catalyst layer by measurement with an integrating sphere on a transparent electrode. The transparent electrode was composed of ALD TiO_2 on FTO (the TiO_2 was necessary as the catalyst did not adhere to the FTO surface). The RuO_x layer behaved as a neutral density filter and gave a weak absorption over the spectral range of the IPCE measurement in Figure 6, resulting in a loss of 8–10% of solar incident power (see Supporting Information). Further optimization of the catalyst thickness may allow for thinner and less absorbing catalyst layers to be used, thus improving overall efficiency.

Although we were confident that hydrogen was generated due to the substantial bubble evolution during photoelectrochemical measurements, we carefully measured the Faradaic efficiency of our photocathode prepared with the RuO_x catalyst. Our method for the hydrogen measurements and efficiency calculations allowed us to monitor any changes in the efficiency that evolve with time (see Supporting Information). Of particular interest to us was the Faradaic efficiency of a photocathode that slowly deactivates, which might give an indication of corrosion. We performed hydrogen measurements on a sample onto which the deposition of catalyst was clearly non-uniform, which tends to yield a less stable photocathode. The measurements were carried out in a gas-tight H-cell under continuous illumination and vigorous stirring to ensure a rapid exchange of hydrogen between the aqueous and gas phase. Hydrogen was measured eight times over the

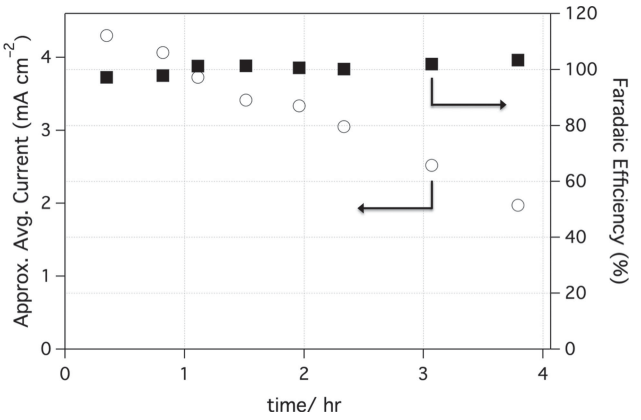

Figure 7. Photocurrent densities and Faradaic efficiency measurements for a photocathode with a non-homogeneous deposition of RuO_x catalyst under continuous illumination at 0 V/RHE in standard pH 5 electrolyte, which confirms ~100% Faradaic efficiency for hydrogen generation even as the photocurrent decays.

course of four hours and we calculated a Faradaic efficiency of 100 ± 2% (**Figure 7**). During these four hours, the photocurrent dropped by more than half, yet we retained unity Faradaic efficiency (within experimental error). These data indicate that the drop in photocurrent with time is likely not due to corrosion. In areas of the photocathode surface where there is none or not enough catalyst, electron trapping in the TiO_2 film can produce states (Ti^{3+}) which promote recombination (this relatively small amount of trapped charge would not be noticed within the experimental error of the Faradaic efficiency measurements). Ti^{3+} ions also absorb visible light and hence filter the incoming photon flux. Thus, effective catalysis can prevent this deleterious electron trapping by allowing the electrons in the TiO_2 film to flow unimpeded into the solution, generating hydrogen.

2.5. Characterization of the ALD TiO_2 Layer

In general, we observed that the photoelectrodes with TiO_2 protective films prepared with hydrogen peroxide as the oxygen precursor showed increased stability versus the films prepared with water as the oxygen source. Even though the RuO_x catalyst layer appears to conformally coat the surface, the high porosity of this layer likely means that the underlying TiO_2 layer remains exposed to the electrolyte. Thus, we characterized the TiO_2 films prepared with the different oxygen precursors to look for differences in crystallinity and/or stoichiometry that may point to a reason for stability differences. X-ray diffraction (XRD) and Raman analysis of the TiO_2 films deposited at 150 °C using TDMAT and either H_2O or H_2O_2 revealed that both films were completely amorphous. Moreover, X-ray photoelectron spectroscopy (XPS) revealed only minor differences in the stoichiometry of Ti and O in the surface region of both films (see Supporting Information).

We characterized the electrical properties of the TiO_2 film prepared with hydrogen peroxide with electrochemical impedance spectroscopy (EIS) and Mott–Schottky analysis to extract

Table 1. Comparison of the Electrical Properties of the Amorphous TiO_2 Films

TiO_2 Oxygen Precursor	E_{fb} (V/RHE)	N_D [cm^{-3}]
water[a)]	–0.12	4.0×10^{20}
hydrogen peroxide[b)]	–0.10	3.5×10^{19}

[a)]Values from reference [14]; [b)]From this work, see Supporting Information.

the flatband potential and donor density (N_D). We carried out the impedance measurement under the same conditions as we previously reported using water as the oxygen precursor[14] in order to make a direct comparison between the two films (see Supporting Information for details). As can be seen in **Table 1**, the flatband potential is the same for both oxygen precursors, and the peroxide film has an order of magnitude lower carrier concentration, although it is still highly doped with a carrier concentration of 3.5×10^{19} cm^{-3}. This lower doping level makes sense as there are less oxygen vacancies expected to be formed when H_2O_2 is used as a source of oxygen dianions compared to pure water. Oxygen vacancies act as donor centers increasing the electron concentration. The donor density of the TiO_2 film has little impact on its performance because the photoelectrons injected from the underlying p–n junction can move in the conduction band. Even poorly doped TiO_2 will easily conduct electrons under these conditions (photo-doping[16]), as long as the film is thin enough to afford screening of the injected electrons by ions located at the TiO_2 surface or by protons intercalated in the titania film. And since the flatband potentials are the same (within experimental error), the comparison of the electrical properties does not offer a clear explanation of the difference in stability that we observe.

2.6. Morphology of the Ruthenium Oxide Catalyst

The most dramatic difference between the photoelectrodes prepared with hydrogen peroxide as the oxygen precursor for the TiO_2 films was the morphology of the deposited RuO_x films. Six samples were prepared from the same batch of cuprous oxide electrodes. Three of the samples were prepared using hydrogen peroxide as the oxygen precursor in the TiO_2 layer and the other three samples were prepared using water as the oxygen precursor. Everything else involved in the preparation was identical, including the same photo-electrodeposition technique for deposition of the ruthenium oxide catalyst. As can be seen in **Figure 8**, the deposited RuO_x catalyst is much more textured and has a higher surface area on the three samples where hydrogen peroxide was used in the TiO_2 layer growth. The electrodes prepared with water appear much smoother by comparison. It should be noted that the ALD TiO_2 layers are conformal and smooth in both cases. This observation suggests an island-growth mechanism in the peroxide case whereas we see a more homogeneous nucleation and growth in the water case. One possible explanation for this dramatic difference in catalyst morphology could be a difference in the TiO_2 surface structure that may result in different nucleation and growth of

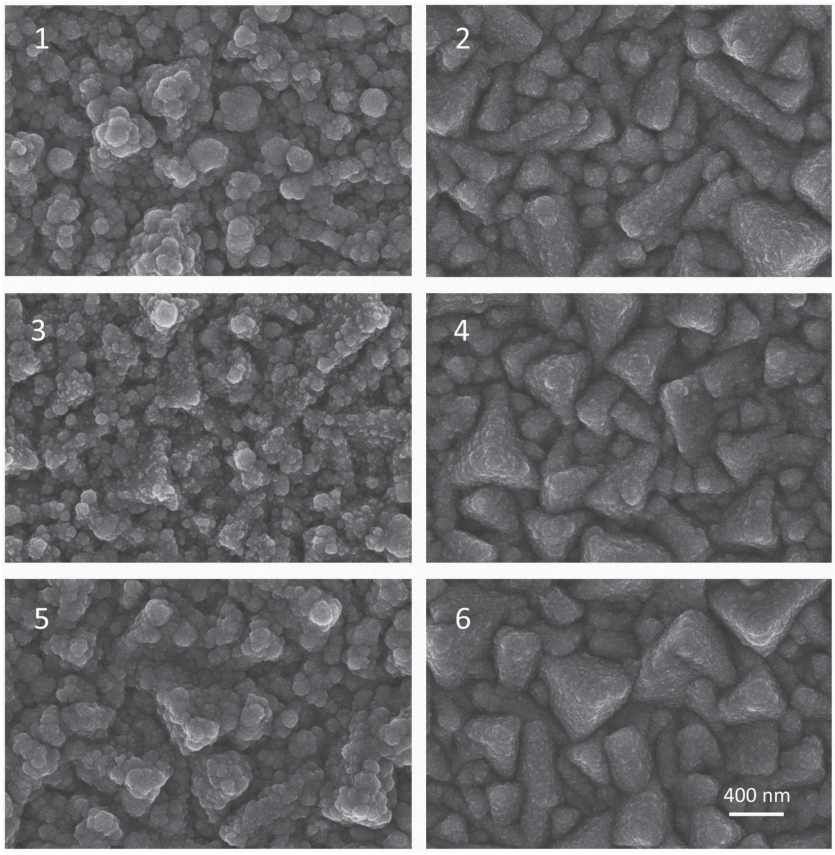

Figure 8. Top-view SEM images of six different electrodes illustrating the difference in catalyst morphology due to growth of the ALD TiO_2 layer with peroxide (left column) and with water (right column). Images in the first row were acquired directly after photoelectrodeposition of the catalyst, but before activation. The middle row shows samples with activated catalyst after a few linear sweeps under illumination and the last row shows samples after several hours of stability measurements. The magnification is the same for all samples.

the RuO_x. However, this hypothesis is difficult to substantiate as we are unable to see any significant differences using the appropriate physical characterization methods (XPS, Raman and XRD). Another possibility, however, is that the difference arises from the differences in the electronic structure of the amorphous TiO_2 films and could be related to the lower electron concentration observed for films made from the H_2O_2 precursor (Table 1).

The higher surface area of the catalyst increases its activity, and the electrons are more efficiently extracted from the TiO_2 underlayer (by facilitating hydrogen evolution through water reduction), thereby avoiding the deleterious electron trapping in the titanium dioxide. If all of the photoelectrons that are generated by the p–n junction flow smoothly into solution with the assistance of better catalysis, the probability of trapping electrons in the TiO_2 layer (likely concomitant with cation intercalation) becomes less, and the stability of the system increases.

3. Conclusions

In order to improve further the performance of this system, we are optimizing the catalyst loading to minimize unproductive light absorption in the catalyst layer and nanostructuring the Cu_2O film, both of which will improve the plateau photocurrents that can be obtained with this system. We also aim to improve photon-to-current efficiency in the wavelength range close to the bandgap. Finally, the protective overlayer will continue to be optimized in order to minimize deleterious electron trapping in the film.

4. Experimental Section

Electrodeposition of Cuprous Oxide: The Cu_2O thin films were deposited by electrodeposition from a basic solution of lactate-stabilized copper sulfate. The substrate for the electrodeposition (working electrode) was TEC-15 F:SnO_2 (FTO, NSG glass) coated with 150 nm of Au, deposited by thermal evaporation with a 10 nm Cr adhesion layer. The plating bath composition has been described previously[13] but the normal electrodeposition time was halved for all of the electrodes used in this work. Thus, a charge of 0.63 C cm^{-2} was passed by applying a current of –0.1 mA cm^{-2} for 105 min, resulting in a Cu_2O thickness of roughly 500 nm, as confirmed by cross-sectional SEM (expect 778 nm based on Coulombs passed and density of Cu_2O, thus ~64% Faradaic efficiency for the one electron reduction of Cu^{2+} in solution to Cu^{+} in the oxide film). On average, decreasing the amount of copper oxide by half had no effect on the onset potential or the fill factor, and sometimes results in higher plateau photocurrents (Figure S1).

Atomic Layer Deposition of Overlayers: Ultrathin layers of n-type oxides were deposited on the surface of the Cu_2O thin films using a thermal ALD system (Savannah 100, Cambridge Nanotech). Prior to ALD, the Cu_2O samples were simply rinsed with DI water and dried under a stream of air. A portion of the exposed gold substrate was masked with Kapton tape prior to deposition of the overlayers. The ALD of Al:ZnO (AZO) was carried out as described previously (20 nm).[14] Titanium dioxide (TiO_2) was deposited at a substrate temperature of 150 °C using tetrakis(dimethylamino)titanium, TDMAT (99.99%, Aldrich), at a precursor temperature of 75 °C, and hydrogen peroxide (50% in water, stabilized, Aldrich) at room temperature. The hydrogen peroxide was stored at 4 °C, and the stainless steel bubbler was charged with fresh, cold hydrogen peroxide solution prior to each deposition of TiO_2, but the precursor solution was allowed to warm to room temperature prior to deposition. TiO_2 was deposited in pulse mode under a nitrogen flow of 5 sccm, with a pulse length of 0.1 s and wait period of 10 seconds for both precursors. The growth per cycle (GPC) for TiO_2 was determined by ellipsometry on a silicon wafer with native oxide and corresponded to 0.58 Å $cycle^{-1}$ at 150 °C.

For one study, the overlayers were deposited directly onto FTO. The FTO was cut into 1×3 cm pieces and then cleaned by sonication sequentially in isopropanol (20 min), soapy water (15 min), distilled water (10 min), and finally isopropanol (5 min). A portion of each substrate was masked with Kapton tape. The substrates were heated to 120 °C in the reaction chamber of the ALD and hydrogen peroxide was pulsed 50 times (0.05 sec pulse time) in order to thoroughly clean the surface. Twenty nanometers AZO were deposited as described previously and then the substrates were heated to 200 °C for the deposition of 50 nm TiO_2 using TDMAT and H_2O_2, utilizing the same conditions as described above for 150 °C. The GPC for TiO_2 was determined by

ellipsometry on a silicon wafer with native oxide and corresponded to 0.61 Å cycle^{-1} at 200 °C. After deposition, the Kapton® tape mask was removed and the exposed FTO was ultrasonically soldered to make a robust connection for the alligator clip.

Catalyst Photoelectrodeposition: For the catalysts used in this study (Pt and RuO_x), the technique of galvanostatic photodeposition was used for the Cu_2O samples (standard dark electrodeposition was used for the FTO only sample). A 1 mM solution of H_2PtCl_6 was used for platinization, and a 1.3 mM solution of $KRuO_4$ was used for deposition of RuO_x. Typically, samples were platinized at a current density of –8.5 μA cm^{-2} for 15 min under simulated one sun illumination (details of light source are described below). A short light chop during the deposition revealed 0.7 V of photovoltage at this small current density (Figure S2). The Cu_2O sample of Figure 5 was modified using the aqueous $KRuO_4$ solution at a current density of –28.3 μA cm^{-2} for 15 min under simulated one sun illumination. A short light chop during the deposition revealed 0.6V of photovoltage through the dark green solution at this current density (Figure S3). It should be noted that even in the dark the cathodic deposition takes place at relatively low voltages (i.e., at voltages that are insufficient for water reduction). E-beam evaporation of platinum was carried out in a Leybold Optics LAB 600H machine, with a nominally 1 nm layer deposited over a period of 10 s.

Photoelectrochemical Characterization: The photoelectrochemical performance of the electrodes was evaluated in a three-electrode configuration using an Ivium Potentiostat/Galvanostat. The samples were interfaced with the PEC cell via an o-ring and a circular aperture designating an illuminated active area of 0.283 cm^2. The electrolyte used was a combination phosphate 0.1 M–Na_2SO_4 0.5 M at pH = 5.0. The reference electrode was Ag/AgCl in saturated KCl, and a Pt wire was used as the counter electrode. The photoresponse was measured under chopped irradiation from a 450 W Xe-lamp (Osram, ozone-free) equipped with an IR/UV filter (KG3 filter, 3 mm, Schott), calibrated with a silicon diode in order to simulate AM 1.5 illumination (100 mW cm^{-2}). The scan rate for the linear sweep voltammetry was 10 mV s^{-1} in the cathodic direction. The electrolyte was sparged with nitrogen for at least 10 min before measurement and was maintained during the measurement as well. IPCE measurements were performed under light from a 300 W xenon lamp with integrated parabolic reflector (Cermax PE 300 BUV) passing through a monochromator (Bausch & Lomb, bandwidth 10 nm FWHM). Comparison with a calibrated Si photodiode allowed the calculation of the IPCE.

Digestion of Deposited RuO_x Catalyst: In order to determine the mass of catalyst present on the sample, RuO_x deposition was carried out on a sample of FTO / 50 nm TiO_2 as described above but for 30 000 s and without illumination, resulting in a homogeneous black deposit. This sample was subsequently digested overnight in approx. 15 mL concentrated HCl at 100 °C, yielding a transparent glass slide. The resulting solution was diluted with 0.1 M HCl to exactly 50 mL and its ruthenium content determined by atomic absorption spectroscopy (Perkin Elmer, AAnalyst 400 Atomic Absorption Spectrometer; Perkin Elmer, Lumina, Ru Hollow Cathode Lamp). Ruthenium chloride hydrate (~41% Ru, Fluka, Switzerland) was used as a standard and an error of 10% was assumed on its Ru content. The ensuing relative error is added to the standard deviation obtained from 5 subsequent atomic absorption measurements, yielding an error of ± 1.1 ppm.

Measurement of Light Absorption by the Catalyst: In order to calculate the losses associated with light absorption by the catalyst, electrodeposition of ruthenium oxide was carried out as described above but without illumination on a sample of TEC-15 FTO / 20 nm TiO_2, yielding a homogeneous darkened area of 1.5 cm^2. Subsequently, the back side of the sample was etched with concentrated HCl in order to remove residual ruthenium impurities. An identical sample without ruthenium oxide was subjected to the same treatment and used as a reference. The total (direct + diffuse) transmission of both samples was measured using a UV/VIS spectrophotometer (Shimadzu UV-3600) equipped with an integrating sphere (Shimadzu, ISR-3100). The spectrum was transformed into fraction of transmitted light and integrated with the AM 1.5 spectrum between 650 and 350 nm to yield the transmitted light energy per square meter. The relative difference between the two values corresponds to the energy lost due to the presence of ruthenium oxide.

Faradaic Efficiency: The faradaic efficiency of the photocathode was measured in a gastight photoelectrochemical H-cell, equipped with a frit separating both compartments and with a quartz window (1.5 cm in diameter). An Ag/AgCl (KCl sat.) reference electrode was employed (Metrohm 6.0724.140) and a platinum wire (Fisher Scientific P/3640/88) was used as counter electrode. Epoxy (LocTite Poxy Pak) was employed in order to mask exposed metal parts of the cathode (active area was 0.77 cm^2) and measurements were performed in the standard electrolyte (combination phosphate 0.1 M–Na_2SO_4 0.5 M, pH = 5.0). The solution in the working compartment was vigorously stirred and constantly sparged with argon (99.998%, Carbagas) at a rate of 3.29 sccm, controlled by means of a mass flow controller (Bronkhorst, Hi-Tec F-201C-FB-22-V). The gas outlet of the working compartment was passed into a 10 cm water column in order to build up a small backpressure. 5 mL gas samples were repeatedly taken at a rate of 2 mL/min by the means of a syringe pump (Sono-Tek Model 997). These samples were subsequently analyzed by gas chromatography (Perkin Elmer AutoSystem, Perkin Elmer Mol. Sieve Column 5 Å 80/100 12' 1/8"). Calibration of the system was achieved by replacing the working electrode with a platinum wire (Fisher Scientific P/3640/88) that was previously treated in a propane flame and running galvanostatic electrolyses at 1, 3, and 5 mA using a EG&G PAR 273A Potentiostat / Galvanostat to generate a calibration curve (four points including the origin, linear fit $R^2 = 0.99983$). For the photocathode measurements, the same optical system was used as for the standard PEC measurements. However, due to the non-standard placement of the H-cell into the beam path, the light intensity was slightly higher than 1 sun and was estimated to lie between 1 and 1.3 suns. An approximate current density is reported as the illuminated area of the photocathode was slightly smaller than the area left accessible by epoxying. In addition to that, the electrode was not perfectly perpendicular to the light beam. However, only the absolute current measurement is necessary for the faradaic efficiency calculation.

Thin Film Characterization: The morphology of the films was characterized using a high-resolution scanning electron microscope (FEI XLF30 SFEG and also a Zeiss Merlin) with a through-the-lens detector for secondary electrons. Cross-sectional images were acquired from freshly cleaved surfaces and were imaged with 5 kV of accelerating voltage. Grazing Incidence X-ray diffraction (GIXRD) patterns were acquired with a Bruker D8 Discover diffractometer, using monochromatic Cu Kα1 radiation (1.540598 Å). The X-ray source was tilted at 1° and the spectra were acquired by moving the linear silicon strip "Lynx Eye" detector between 2θ = 20° and 2θ = 65° at a scan rate of 0.06 deg/min with step width of 0.02°. Reflection patterns were matched to the PDF-4+ database (ICDD).

Raman scattering measurements were made using a 532 nm wavelength laser beam and were acquired with a Labram HR800 model of Jobin-Yvon Horiba spectrometer equipped with a microscope for collection of backscattered Raman signals.

XPS data were collected with an Axis Ultra (Kratos Analytical) using a monochromatic Al K-alpha X-ray source (1,486.6 eV).

Supporting Information

Supporting Information is available from the Wiley Online Library or from the author. Available are: J–V curves of photocathodes with different thicknesses of Cu_2O, chronovoltammetry plots of catalyst photoelectrodeposition, top-view SEM image of photocathode after long-term stability measurement, Mott–Schottky plot and XPS data of the TiO_2 film.

Acknowledgements

We thank the Swiss Federal Office for Energy (PECHouse Competence Center, contract number SI/500090–02), the European Commission

(Project NanoPEC – Nanostructured Photoelectrodes for Energy Conversion, contract number 227179), the Energy Center at EPFL, the SNF, and NCCR MUST for financial support. João Azevedo is thankful to FCT SFRH/BD/79207/2011 and PTDC/EQU-EQU/107990/2008 for a PhD grant. We also thank Dr. Nicolas Tétreault and Mr. Aravind Chandiran (Laboratory of Photonics and Interfaces, EPFL) for carrying out the ellipsometric measurements, Dr. Thomas Moehl (Laboratory of Photonics and Interfaces, EPFL) for helpful discussions regarding the EIS measurements, and Prof. Kevin Sivula (Laboratory for Molecular Engineering of Optoelectronic Nanomaterials, EPFL) for use of his integrating sphere. Additionally, we thank Véronique Amstutz and Prof. Hubert Girault (Laboratory of Physical and Analytical Electrochemistry, EPFL) for the use of their GC for the hydrogen measurements, Nicolas Xanthopoulos from the Centre Interdisciplinaire de Microscopie Electronique (CIME) at EPFL for the XPS measurements, as well as Stéphane Thonney and Christophe Roussel for their assistance with the AAS measurements.

Received: March 29, 2013
Revised: June 20, 2013
Published online: July 16, 2013

[1] P. J. Boddy, *J. Electrochem. Soc.* **1968**, *115*, 199–203.
[2] A. Fujishima, K. Honda, *Nature* **1972**, *238*, 37–38.
[3] M. G. Walter, E. L. Warren, J. R. McKone, S. W. Boettcher, Q. X. Mi, E. A. Santori, N. S. Lewis, *Chem. Rev.* **2010**, *110*, 6446–6473.
[4] K. J. Young, L. A. Martini, R. L. Milot, R. C. Snoeberger, V. S. Batista, C. A. Schmuttenmaer, R. H. Crabtree, G. W. Brudvig, *Coord. Chem. Rev.* **2012**, *256*, 2503–2520.
[5] C.-Y. Lin, Y.-H. Lai, D. Mersch, E. Reisner, *Chem. Sci.* **2012**, *3*, 3482–3487
[6] Z. Zhang, P. Wang, *J. Mater. Chem.* **2012**, *22*, 2456–2464
[7] P. D. Tran, S. K. Batabyal, S. S. Pramana, J. Barber, L. H. Wong, S. C. J. Loo, *Nanoscale* **2012**, *4*, 3875.
[8] Y. Mao, J. He, X. Sun, W. Li, X. Lu, J. Gan, Z. Liu, L. Gong, J. Chen, P. Liu, Y. Tong, *Electrochim. Acta* **2012**, *62*, 1–7.
[9] A. A. Aref, L. Xiong, N. Yan, A. M. Abdulkarem, Y. Yu, *Mater. Chem. Phys.* **2011**, *127*, 433–439.
[10] L. Wu, L. Tsui, N. Swami, G. Zangari, *J. Phys. Chem. C* **2010**, *114*, 11551–11556.
[11] L. Chen, S. Shet, H. Tang, H. Wang, T. Deutsch, Y. Yan, J. Turner, M. Al-Jassim, *J. Mater. Chem.* **2010**, *20*, 6962.
[12] A. Paracchino, V. Laporte, K. Sivula, M. Gratzel, E. Thimsen, *Nat. Mater.* **2011**, *10*, 456–461.
[13] A. Paracchino, J. C. Brauer, J.-E. Moser, E. Thimsen, M. Graetzel, *J. Phys. Chem. C* **2012**, *116*, 7341–7350.
[14] A. Paracchino, N. Mathews, T. Hisatomi, M. Stefik, S. D. Tilley, M. Graetzel, *Energy Environ. Sci.* **2012**, *5*, 8673–8681.
[15] E. R. Kötz, S. Stucki, *J. Appl. Electrochem.* **1987**, *17*, 1190–1197.
[16] M. Grätzel, *Inorg. Chem.* **2005**, *44*, 6841–51.
[17] B. Seger, T. Pedersen, A. B. Laursen, P. C. K. Vesborg, O. Hansen, I. Chorkendorff, *J. Am. Chem. Soc.* **2013**, *135*, 1057–64.
[18] J. Brillet, J. Yum, M. Cornuz, T. Hisatomi, R. Solarska, J. Augustynski, M. Graetzel, K. Sivula, *Nat. Photonics* **2012**, *6*, 824–828.
[19] H. Over, *Chem. Rev.* **2012**, *112*, 3356–426.
[20] S. Trasatti, *Electrochim. Acta* **2000**, *45*, 2377–2385.
[21] A. Mills, P. A. Duckmanton, J. Reglinski, *Chem. Commun.* **2010**, *46*, 2397.